Microwave Induced Qubit Resonator Coupling

Sina Zeytinoğlu
Semesterarbeit , Department of Physics, ETH Zürich

September 26, 2013

Abstract

A tunable coupling between a qubit and its host resonator is desired for the implementation of quantum information processing applications related to entanglement distribution over distant atoms [1, 2]; and the demonstration of effects due to adiabatic quantum processes such as the vacuum induced Berry phase [3]. In this semester thesis, we realize the desired tunable coupling via a cavity assisted Raman process implemented in a multilevel transmon qubit coupled to a single resonator mode. By virtue of being induced by an external microwave drive, the Raman process provides an effective coupling between the qubit and the resonator whose strength $\tilde{g}$ is tunable both in amplitude and phase. We provide experimental data and numerical simulations characterizing the process. We also provide a perturbative treatment to approximate the effective coupling strength $\tilde{g}$ and fidelity F of the Raman transition.

Contents

1 Motivation

In this semester thesis, we will analyze a second-order off-resonant (Raman) process between $|f0\rangle$ and $|g1\rangle$ states of a multi-level transmon qubit [15] coupled to a single resonator mode. The Raman transition is enabled by the combination of the qubit-resonator coupling with strength g_n and external drive with strength Ω_n (Fig. 1).

There are two main motivations for this thesis. First, we would like to demonstrate the phase and amplitude tunability of qubit-resonator coupling via a two photon Raman process and measure the dependence of the coupling rate to the external drive frequency and strength.

Second, we would like to create a simple toolbox to efficiently predict the effective coupling strength $\tilde{g}$ and the fidelity F of cavity assisted[1] Raman transitions in transmon qubits.

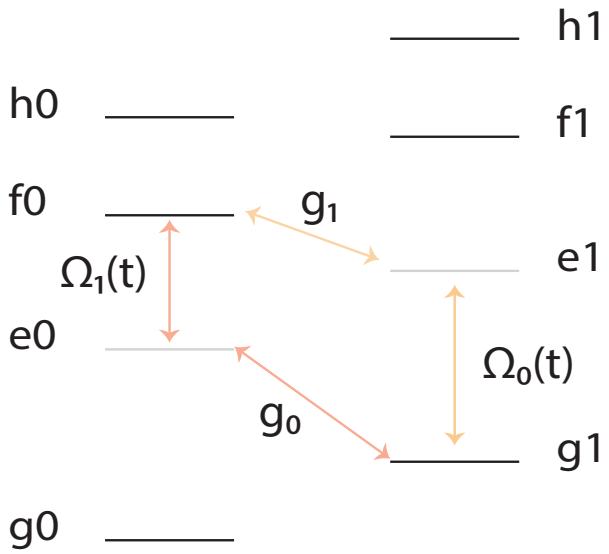

Figure 1: The two second order transition paths through which the Raman process between $|f0\rangle$ and $|g1\rangle$ can occur. The strength of interactions due to the qubit-resonator coupling and the external drive are denoted by $g_n = g_0\sqrt{n+1}$ and $\Omega_n = \Omega\sqrt{n+1}$, respectively. Subscript n denotes the smallest number of excitations in the qubit for states coupled by the external drive; and one less than total number of excitations for states coupled by the qubit-resonator coupling.

1.1 Applications

A qubit-resonator coupling that is tunable both in amplitude and phase ($\tilde{g}$) is desired for experiments both in fundamental and applied physics.

On the applied side, tunable amplitude and phase of $\tilde{g}$ plays the central role in "photon shaping" experiments, in which one wants to tailor the wavepacket of a single photon to optimize the transmission of information between two distant qubits. A proposal by Cirac et. al. [1] shows that it is possible to establish perfect communication between two distant quantum systems if the transmission is mediated by photons with time-reversal symmetric

[1] Cavity assisted means that one of the two coupling contributing to the Raman transition is the qubit-resonator coupling g

wavepackets. The main idea of the proposal is that if a photon's wavepacket is time-reversal symmetric, it will be emitted by one of the quantum systems the same way it is absorbed by the other, allowing perfect transmission of quantum information. The implementation of perfect transmission protocol is a big step towards the "Quantum Internet" [2] in which the distant quantum systems, so called "nodes", share and process quantum information. When realized, the "Quantum Internet" will allow quantum computation at large scales.

Another application of the phase tunability of $\tilde{g}$ is in fundamental physics and is related to the demonstration of the "Vacuum Berry Phase" [3] in a solid state cavity QED setting. As in the previous demonstrations of the Berry phase in superconducting qubits [4, 5], the qubit-resonator ground state is adiabatically transported around a closed loop on the Bloch sphere representing the two-level system. The non-trivial topology of the two-level system allows a non-zero geometric phase (i.e. Berry phase), which is directly proportional to area enclosed by the closed loop. In the previous experiments, however, the adiabatic transport was enabled by varying the phase of the coherent drive amplitude α as in the Rabi model. Thus, the acquired Berry phase results from qubit's interaction with many photons in a coherent superposition. On the other hand, the "Vacuum Induced Berry Phase" is due to the interaction of the qubit with a 1 photon state $\big(|g1\rangle$ for our experiments$\big)$, and thus the Berry phase acquired is due to the geometric evolution of the system under a quantized field [2][6]. Such a transition requires a phase tunable qubit-cavity coupling, which is possible with the Raman process subject to this thesis.

Moreover, Raman transitions [3] are one of the building blocks of quantum information science using atoms [7]. The large anharmonicity of the atomic energy levels ($\approx$ 1 GHz) and the abundance of dipole forbidden transitions allow the treatment of the problem as an effective three level system in Λ or a ladder-type Ξ configuration [8]. The most common method for calculating the dynamics of these three level systems is "adiabatic elimination", which relies on the condition that the two drive strengths Ω_1 and Ω_2 are much smaller than the detuning of the drive frequencies Δ with respect to their target transition frequencies. This condition also entails that the intermediate levels in the Raman transition are not significantly populated.

However, for superconducting transmon qubits, the ratio between the anharmonicity ($\alpha/2\pi \approx 200$ MHz) and the typical drive strengths ($\Omega/2\pi \approx 100$ MHz) is much closer to 1, and the adiabatic elimination procedure fails to give satisfactory results. Other difficulties with the adiabatic elimination scheme has been previously pointed out and new approaches has been provided [11, 12]. In this thesis, we will also present a technique which can be used instead of adiabatic elimination, and gives higher accuracy which is desired to explain experiments involving higher order transitions in transmon qubits.

2 Introduction

In this thesis, we consider a quantum system consisting of a transmon qubit and a single mode of the superconducting resonator. The Hamiltonian[4] of this system is given by

[2]However, in principle, since the Raman process is induced by a coherent drive, the transmon qubit is still interacting with many photons

[3]In contrast to their cavity assisted cousins, Raman transitions in atomic physics are induced by two separate coherent drives, possibly with different frequencies, strengths and polarizations [9, 10].

[4]For simplicity, the resonator drive (which is used for qubit readout [13]) and resonator anharmonicity terms are neglected. When included, the resonator and the qubit enter the exact same way in the Hamiltonian.

$$H/\hbar = \omega_q a^\dagger a + \alpha b^\dagger b^\dagger b b + \omega_r \hat{n}_r + \Omega \cos(\omega_d t + \phi)(b + b^\dagger) + g(ba^\dagger + b^\dagger a). \quad (1)$$

Here, a, $a^\dagger$ and b, $b^\dagger$ are the annihilation and creation operators for the resonator and the qubit, respectively. Also, $\omega_{q(r)}/2\pi$ is the qubit (resonator) frequency, and α is the qubit anharmonicity. In the last two interaction terms, Ω and g stand for the complex valued strengths of the qubit drive and the Jaynes-Cummings couplings, respectively.

In the absence of interactions ($\Omega, g = 0$) the eigenstates of the system can then be expressed as the tensor-product of the bare qubit and resonator eigenfunctions. We denote these functions as $|q\rangle \bigotimes |r\rangle \equiv |qr\rangle$. Since the qubit and the resonator are both discrete systems, q and r denote integer numbers corresponding to the number of excitations in the qubit and the resonator, respectively. The energy level diagram of the system above is shown in Fig. 2.

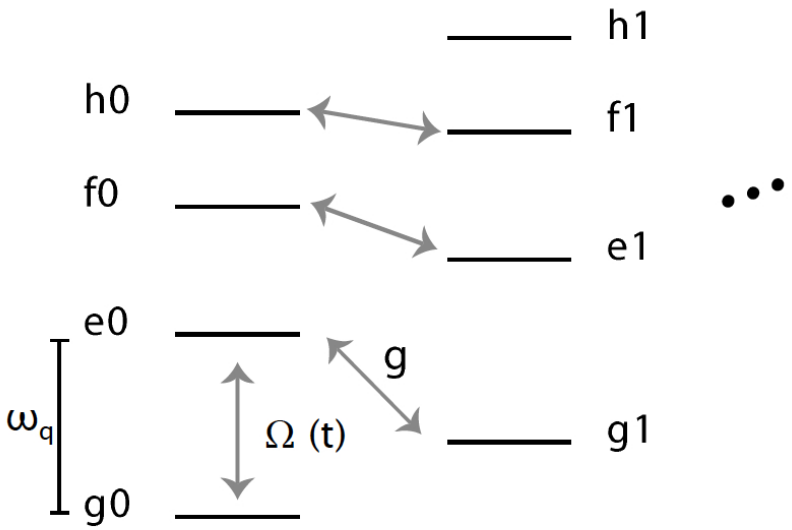

Figure 2: The energy level diagram of a quantum system consisting of a four level transmon qubit and a single resonator mode. The arrows indicate some of the first order transition paths. Ω and g are the associated transition strengths.

Here we note that the interactions induced by Jaynes Cummings coupling, $g(ba^\dagger + b^\dagger a)$, and the external drive, $\Omega \cos(\omega_d t + \phi)(b + b^\dagger)$, couple different set of states. According to Eqn. (1), the Jaynes Cummings coupling conserves the number of excitations, whereas in the case of external drive, only the number of excitations in the resonator mode are conserved (i.e. $|q, r\rangle \rightarrow |q + n, r\rangle$, $n \neq 0$).

Another important difference between the transitions induced by the external drive and Jaynes Cummings coupling is the degree of control one has over the complex amplitudes Ω and g. Although the experimentalist has a good control over both amplitude and phase of the external drive strength Ω, the same is not true for g. In standard circuit QED experiments using transmon qubits the Jaynes Cummings coupling strength g is fixed during the sample fabrication by the relation [15],

$$\hbar g = 2e\beta V^0_{rms} \langle e0 | b^\dagger b | g1 \rangle, \quad (2)$$

where β is the ratio between the gate capacitance and the total capacitance of the qubit-resonator system. As a result, it is impossible to turn the qubit-cavity interaction on and off in a dynamical fashion[5]. As discussed in the previous section, in this thesis, we will investigate the use of a Raman transition to overcome this difficulty.

The organization of this report is as follows. In Section 3, we present the measurement procedure and the measurements of the effective coupling strength of the Raman transition between $\left|f0\right\rangle$ and $\left|g1\right\rangle$. In Section 4, we use perturbation theory to predict the dependencies of the effective coupling $\tilde{g}$ and the fidelity F of the Raman transition on the experimentally tunable parameters. In Section 5, we support the experimental and theoretical results with numerical simulations.

3 Experimental

We used the experimental setup depicted in Fig. 3 to investigate the dependence of $\tilde{g}$ on the system parameters.

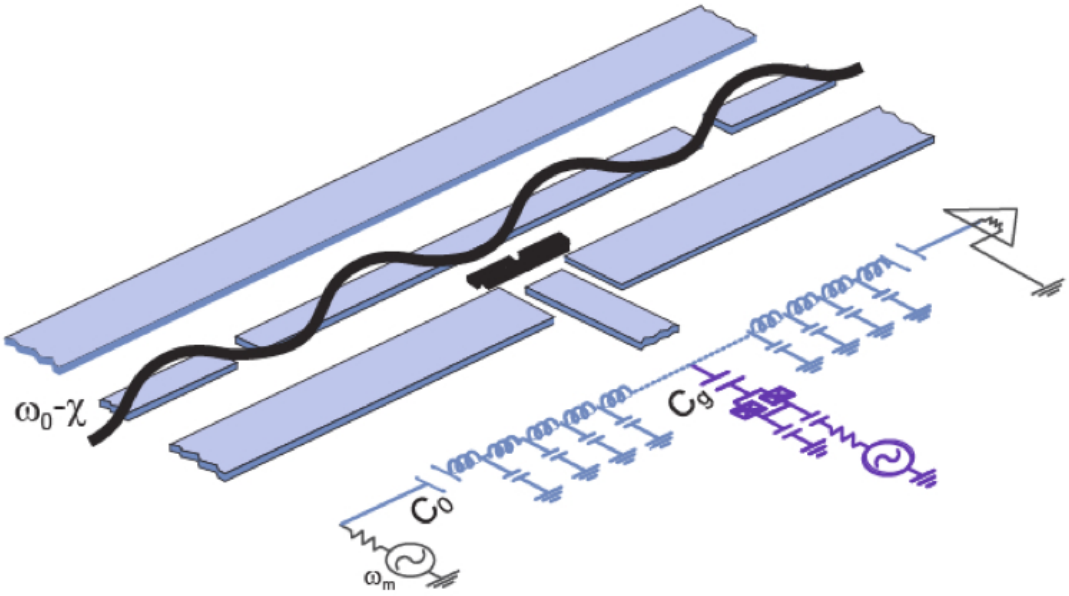

Figure 3: A schematic of the measurement setup and its equivalent circuit. The resonator and qubit frequencies are measured via the resonator transmission. χ represents the qubit state dependent shift in the resonator frequency. C_0 and C_g are the capacitances coupling the resonator to the drive source and the qubit to the resonator, respectively.

3.1 Qubit and Resonator Characteristics

The qubit and the resonator were characterized separately using transmission spectroscopy of the resonator [13]. Transmission spectroscopy is a way to measure the resonator's response to

[5]Although it is possible to tune the coupling between qubit and resonator states by tuning the qubit transition frequency in and out of resonance with the resonator frequency [14] with this method one cannot control the phase of g.

a small perturbing electric field. The resonator is connected to the environment capacitively (C_0) through two ports as shown in Fig. 3. One of these ports is used to drive the resonator with the small drive field with a fixed frequency and amplitude, and the other is used to measure the resonator's response. The data displayed in Fig. 4 is taken by sweeping the resonator drive frequency while keeping its amplitude fixed. Being a damped harmonic oscillator, the bare resonator's response function is a single Lorentzian centered at the resonator frequency, $\omega_r/2\pi = 7.126$ GHz. The full width half maximum of the peak is given by the resonator decay rate $\kappa/2\pi = 10$ MHz. Because the resonator frequency shifts slightly as a function of the qubit transition frequency, we calibrated the resonator after adjusting the qubit transition frequency, ω_q, using the external flux line.

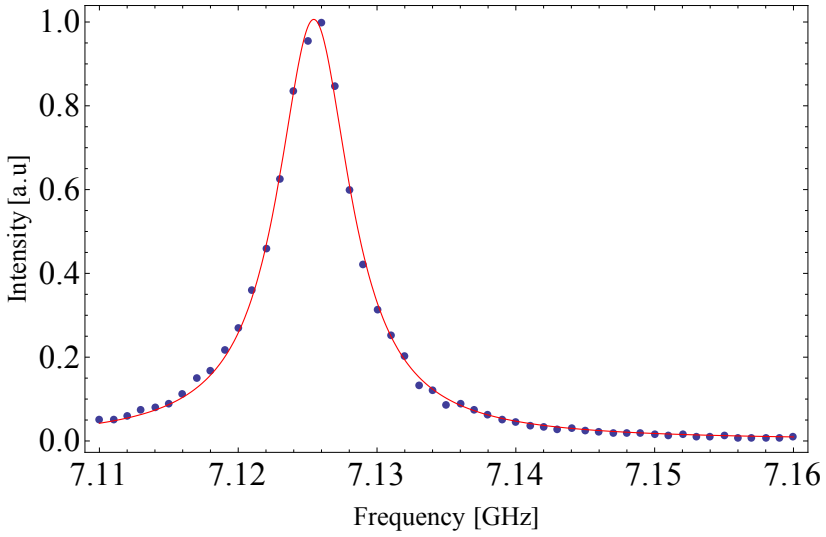

Figure 4: The response function of the bare resonator obtained via resonator transmission. The bare resonator frequency, $\frac{\omega_r}{2\pi}$, is found to be 7.126 GHz.

The calibration of the qubit was also done using transmission spectroscopy of the resonator. The measurement principle makes use of qubit-state dependent dispersive shift of the resonator frequency. For this experiment, we drive the resonator with a fixed amplitude at its resonance frequency, where the resonator response is at its maximum. Dispersive measurement means that the resonator frequency used for spectroscopy is far off-resonant from the qubit transition frequency, $\omega_q/2\pi$. Meanwhile, the qubit is driven capacitatively by another source, shown in purple in Fig 3. When the qubit is driven at its transition frequency, using this on-chip drive, the oscillations between the qubit ground and excited states attenuates the resonator response because of the state-dependent dispersive shift induced on the resonator frequency. This attenuation results in a dip in the resonator response as a function of the qubit drive frequency (Fig. 5). Using this measurement principle, the $\omega_{eg}/2\pi$ frequency is found to be 8.103 GHz[6]. This gives us a qubit resonator detuning of , $\Delta/2\pi = 979$ MHz.

[6]The transmon qubit transition frequency can be adjusted by varying the magnetic flux that goes through the split-pair of Josephson junctions by changing the voltage, V, applied across the solenoids positioned close to the sample. The transition frequency separating the ground and excited states of the transmon qubit depends on the flux through the Josephson junction in accordance with the equation

$$\hbar\omega \approx \sqrt{8E_J E_C}$$

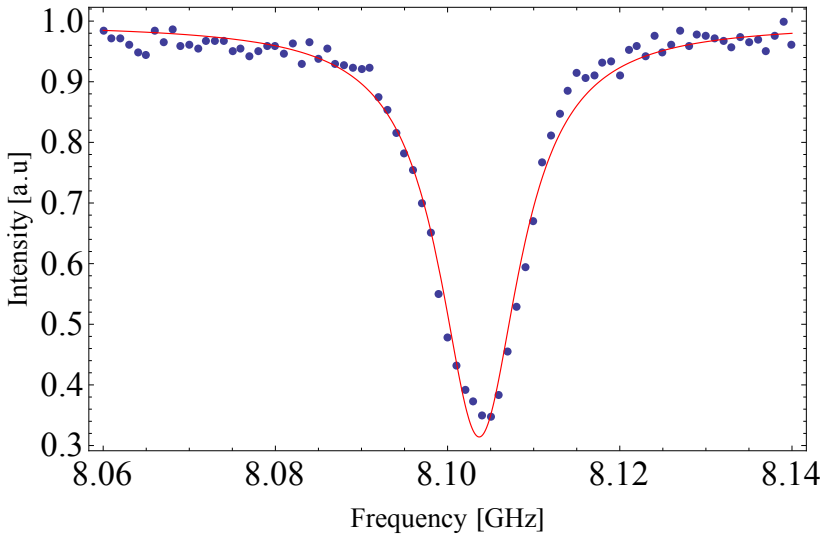

Figure 5: The transmission dip in the resonator signal. The center of the Lorentzian gives the qubit frequency, $\frac{\omega_q}{2\pi}$, which is found to be 8.103 GHz.

Lastly, the anharmonicity of the qubit was determined via the second order transition between ground and 2^{nd} excited states. The transition frequency ω_{gf} obeys the equation

$$\omega_{gf} = \omega_q - \frac{\alpha}{2}, \tag{3}$$

in words, the difference in frequency between the qubit transition frequency, $\omega_q/2\pi$, and the $|g\rangle$ to $|f\rangle$ transition frequency gives half the anharmonicity. The transmission dip corresponding to this transition is shown in Fig. 6.

$\frac{\omega_r}{2\pi}$	7.126 GHz
$\frac{\omega_q}{2\pi}$	8.103 GHz
$\frac{\Delta}{2\pi}$	0.979 GHz
$\frac{\alpha}{2\pi}$	0.376 GHz

Table 1: Characteristic frequencies of the qubit-resonator system.

3.2 Measurement of the Vacuum Rabi Splitting

The coupling strength of the Raman process, $\tilde{g}$, is measured from the splitting of the Lorentzian peak of the resonator response (Fig. 7). The measurement principle is the same as the one used to determine the ω_{eg}, but in this case we fix the qubit drive frequency and sweep the frequency of the resonator drive.

, where $E_J = E_J^{max}\left|\cos(k.V)\right|$ [16]. The constant k can be determined from using at least three values for V when the qubit and the resonators frequencies cross each other, which is seen as an avoided crossing in the resonator response. Once k is calibrated, the qubit transition frequency can be set to a desired value.

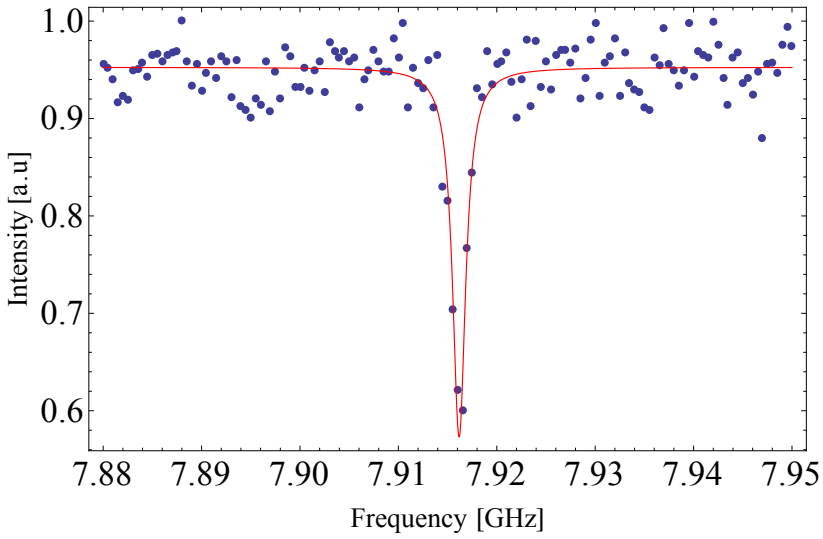

Figure 6: The transmission dip in the resonator signal. The center of the Lorentzian gives half the frequency of $|g0\rangle$ to $|f0\rangle$ transition, $\frac{\omega_{g0f0}}{2\pi}$, which is found to be 0.376 GHz.

The reason for this splitting can be understood as follows. The effective interaction between the $|g1\rangle$ and $|f0\rangle$ states will result in two polariton states

$$|\Phi^{\pm}\rangle,^{7}$$

which are the eigenstates of the total Hamiltonian. In 2^{nd}-order degenerate perturbation theory (See Appendix B), the energies of the polariton states are given by

$$E_{\pm}^{(1)} = \frac{1}{2}\left(\chi_{f0} + \chi_{g1} \pm \sqrt{(\chi_{f0} - \chi_{g1})^2 + 4\tilde{g}^2}\right), \tag{4}$$

where χ_{g1} and χ_{f0} are the AC Stark shifts induced on $|g1\rangle$ and $|f0\rangle$, and $\tilde{g}$ is the transition strength of the Raman transition. The associated eigenstates can be written as $|\Phi^{\pm}\rangle = c_1^{(0)}|f0\rangle + c_2^{(0)}|g1\rangle$, where the 0^{th} order coefficients are

$$c_1^{(0)} = \left(\frac{\tilde{g}}{2|\tilde{g}|}\left(1 \pm \frac{\chi_{f0} - \chi_{g1}}{\sqrt{(\chi_{f0} - \chi_{g1})^2 + 4|\tilde{g}|^2}}\right)\right)^{1/2}, \tag{5}$$

$$c_2^{(0)} = \pm\left(\frac{\tilde{g}}{2|\tilde{g}|}\left(1 \mp \frac{\chi_{f0} - \chi_{g1}}{\sqrt{(\chi_{f0} - \chi_{g1})^2 + 4|\tilde{g}|^2}}\right)\right)^{1/2}. \tag{6}$$

Because the one photon resonator state $|g1\rangle$, overlaps significantly with the two different eigenstates $|\Phi^{\pm}\rangle$ of the qubit-resonator system, we expect the resonator response to be peaked at two distinct frequencies $E_{\pm}/\hbar$.

[7] More accurately, the interaction that causes the splitting is the one between the dressed states, which are discussed and denoted as $|\widetilde{g1}\rangle$ and $|\widetilde{f0}\rangle$ in Section 3.

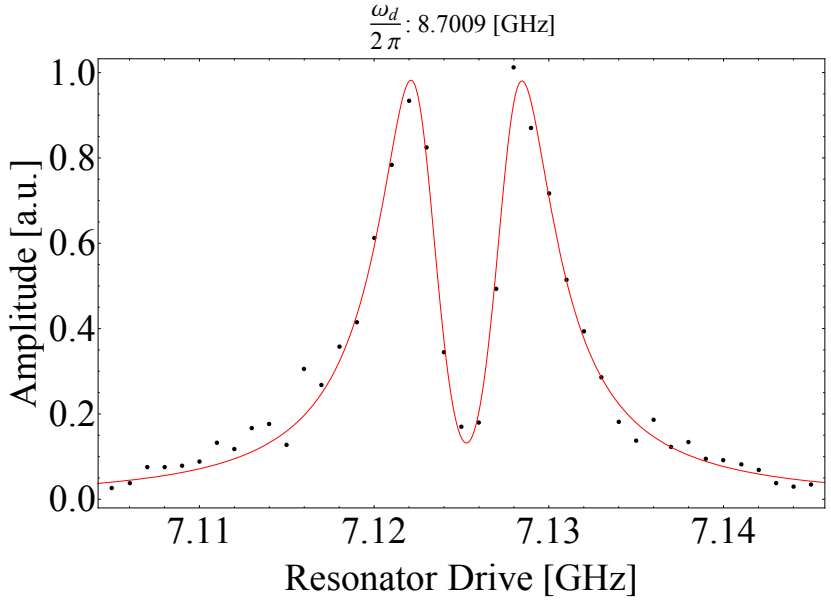

Figure 7: The resonator response function obtained via resonator transmission, when qubit drive frequency was picked such that state $|f0\rangle$ and $|g1\rangle$ are energetically degenerate. The Lorentzian peak of the bare resonator response is split into two peaks separated by a frequency difference of $2\tilde{g}$ when the width of the two peaks are approximately same. The $\tilde{g}$ extracted from this trace is 2.8 MHz

In order to determine $\tilde{g}$, we first measure the resonator response as a function of the qubit and resonator drive frequencies. The sweeps of these two variables results in the 3D data set shown in Fig. 8. In addition, Fig. 7 shows the slice of this 3D data along the axis of constant drive power with drive frequency, $\omega_d/2\pi = 8.7$ GHz. For this configuration, we find the qubit-drive detuning, $\delta_q/2\pi = \omega_q/2\pi - \omega_d/2\pi$ = -0.6 GHz.

According to Eqn. 4, in the case

$$\chi_{f0} = \chi_{g1}, \tag{7}$$

the 0^{th} order coefficients become

$$|c_1^0| = \pm|c_2^0| = \pm 1/\sqrt{2}. \tag{8}$$

As a result, we can extract the value of $\tilde{g}$ directly from the splitting between the two transmission peaks when $|g1\rangle$ overlaps equally with both $|\Phi^+\rangle$ and $|\Phi^-\rangle$. Experimentally, this condition is equivalent to widths of the two transmission peaks being equal. For all other cases, the FWHM of one of the peaks will be closer to the resonator decay rate κ and the other closer to qubit decay rate γ. The FWHM of the polariton peak is given by

$$\Gamma^{\pm} = \left(\frac{1}{\kappa} + \frac{1}{\gamma}\right)^{-1}. \tag{9}$$

Note that the transmission peaks cannot be fitted to two Lorentzians separated by $2\tilde{g}$, since in the regions that the two peaks overlap, they interfere de-constructively. It is possible to understand this interference using 2^{nd} order perturbation theory (See Appendix B).

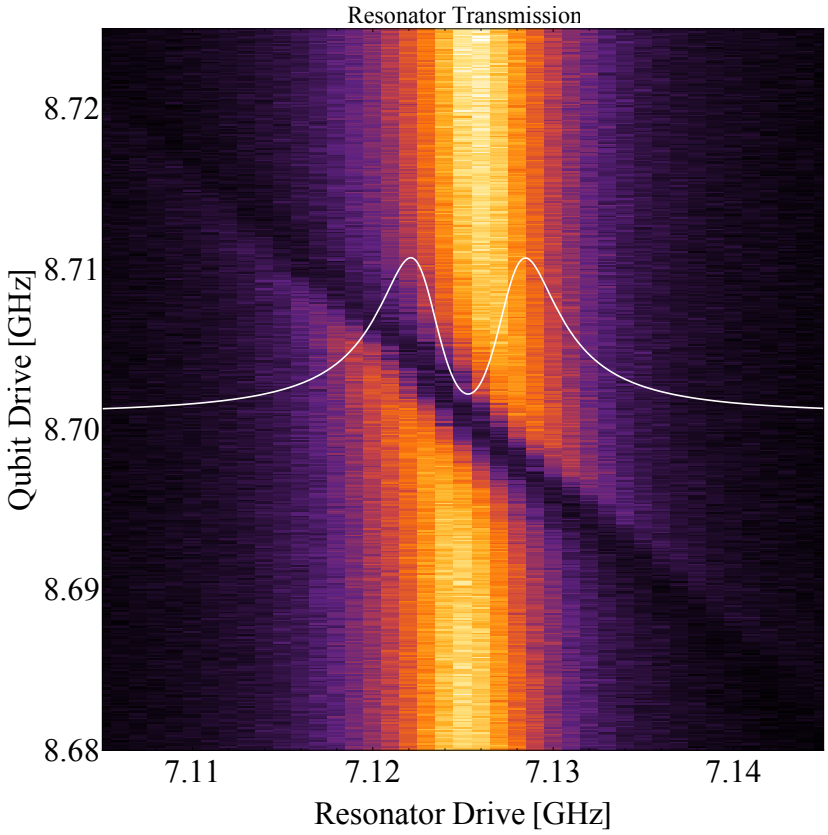

Figure 8: The resonator response as function of qubit and resonator drive frequencies. The white curve is the fit on the slice of data along a fixed qubit drive frequency $\omega_d = 8.7$ GHz.

Consider the transition paths connecting the states describing the input and output ports of the resonator ($\left|in\right\rangle$ and $\left|out\right\rangle$) through intermediate states $\left|\Phi^{\pm}\right\rangle$. The transition strength is proportional to

$$\sum_{i=+,-} \frac{\left\langle out\right|V\left|\Phi^i\right\rangle\left\langle\Phi^i\right|V\left|in\right\rangle}{E_{res} - E_{\Phi^i}},$$

which is attenuated when the resonator is placed in between $\left|\Phi^{\pm}\right\rangle$ because of the opposite signs of the detuning between the resonator and the two intermediate states.

We used a simple classical model of two coupled damped harmonic oscillators to fit the experimental data. The equations of motion for this system is simply

$$2\omega_q \tilde{g} r_r = \omega_q^2 r_q + \ddot{r}_q + \Gamma \dot{r}_q \quad (10)$$

$$A_0 e^{i\omega t} + 2\omega_r \tilde{g} r_q = \omega_r^2 r_r + \ddot{r}_r + \kappa \dot{r}_r, \quad (11)$$

where operator V couples the qubit-resonator states to the input and output ports[8]. is given

[8]The interaction between the resonator and the ports can be written as

$$V = \frac{1}{2}\left(\kappa b(a_{in}^{\dagger} + a_{out^{\dagger}}) + \bar{\kappa} b^{\dagger}(a_{in} + a_{out})\right)$$

, where κ and $\bar{\kappa}$ are the coupling strengths between the resonator and the output and input ports respectively

by $\frac{\kappa}{2}$()where $\omega_q/2\pi$ and $\omega_r/2\pi$ are the transition frequency of the qubit and the fundamental frequency of the resonator. Thus, r_q and r_r describe the charge in the transmon qubit and voltage in the resonator, respectively. The resonator driven by an external drive with an arbitrary amplitude A_0, and the damping terms describe the lifetime of the qubit (γ^{-1}) and the resonator (κ^{-1}). Dephasing of the qubit is not included in this model.

The coupled equations can be solved using the linear response ansatz $r_q = r_{q0}(\omega)e^{i\omega t}$ and $r_r = r_{r0}(\omega)e^{i\omega t}$. We also set the qubit and the resonator on resonance, $\omega_q/2\pi = \omega_r/2\pi = \omega_0/2\pi$, in accordance with the experimental configuration. We can solve the coupled equations for r_r, which corresponds to the voltage output of the resonator. Taking the square of the result gives us the output power which we measure at the output port

$$S(\omega) = A_0^2 \left| \frac{i\,|\Gamma|\,\omega - \omega^2 + \omega_0^2}{4g^2\omega_0^2 - (i\,|\Gamma|\,\omega - \omega^2 + \omega_0^2)(i\,|\kappa|\,\omega - \omega^2 + \omega_0^2)} \right|^2 . \tag{12}$$

By fitting $S(\omega)$ to the trace in which the two peaks are approximately of the same width, we extract the parameters $\tilde{g}$, and Γ. The results are shown in Fig. 9, with a fit to the theoretical model shown in red. The drive power is presented in arbitrary units converted from the power (in dBm) as read from Arbitrary Waveform Generator (AWG), because the losses between AWG and the sample were not properly calibrated[9].

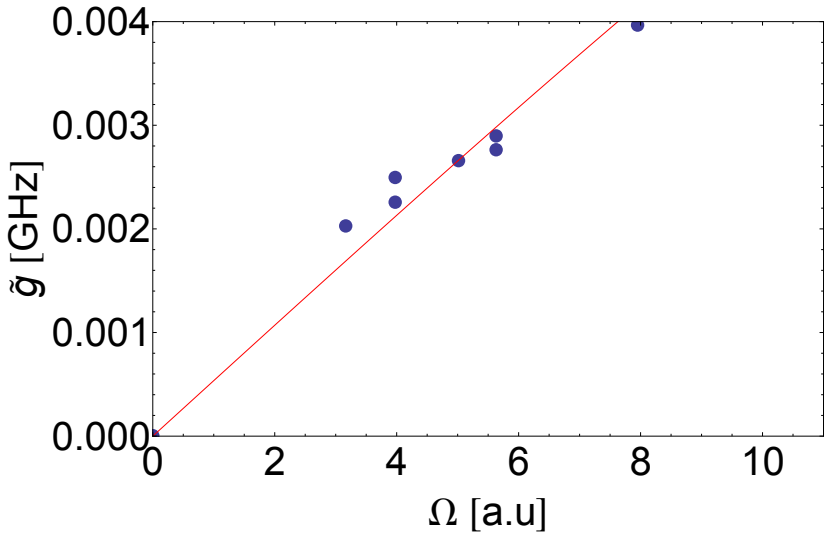

Figure 9: The dependence of $\tilde{g}$ extracted from the fits on the qubit drive power Ω. The fit line uses Eqn. (18), with a the scale of Ω as the fit variable.

[9]An estimation of the losses considering the coaxial cables, thermalizing attenuators, and the factor β in Eqn. (2) would give a large uncertainty which would not give a reasonable test of validity for the calculated $\tilde{g}$ in Eqn. (19). We intend to work on calibrating the drive power reaching the qubit in the future.

4 Theoretical Predictions

4.1 Coupling Strength of Raman Process

In this section we will derive the formulas describing the dependence of $\tilde{g}$ on the qubit drive strength Ω, anharmonicity α, and qubit-resonator coupling strength g. To this end, we use time independent perturbation theory[10] (See Appendix B). We notice that the Hamiltonian of the system can be written as

$$H = H_0 + H', \tag{13}$$

Where H_0 denotes the Jaynes-Cummings Hamiltonian whose exact solution is known, and H' denotes the interactions due to the external qubit drive, which we will treat perturbatively. The Jaynes-Cummings Hamiltonian in the rotating frame is given by:

$$H_0/\hbar \cong \delta q \hat{n}_q + \alpha b^\dagger b^\dagger b b + \delta_r \hat{n}_r + g(b a^\dagger + b^\dagger a), \tag{14}$$

where $\delta_q = \omega_{ge} - \omega_d$ is the difference between the qubit transition frequency between the ground (g) and excited (e) states. Operators a and b are annihilation operators for the resonator and the qubit degrees of freedom, respectively, and $\hat{n}_r$ and $\hat{n}_q$ are the corresponding number operators. The Jaynes-Cummings Hamiltonian can be solved exactly. On the basis of bare eigenstates of the qubit-resonator system (denoted by $\big|n, m\big\rangle$ where n and m are the number of excitations in the qubit and the resonator, respectively), the eigenfunctions can be expended as

$$\big|\Phi_n^+\big\rangle = \cos(\alpha_n)\big|n, m\big\rangle + \sin(\alpha_n)\big|n-1, m+1\big\rangle \tag{15}$$
$$\big|\Phi_n^-\big\rangle = \cos(\alpha_n)\big|n-1, m+1\big\rangle - \sin(\alpha_n)\big|n, m\big\rangle, \tag{16}$$

where α is defined as $\alpha_n = \arctan(\frac{g\sqrt{n}}{\delta_n})$, with $\hbar\delta$ denoting the energy difference between states $\big|n, m\big\rangle$ and $\big|n-1, m+1\big\rangle$. We shall use this set of eigenbases for the Jaynes-Cummings Hamiltonian to construct a time independent perturbation theory for the external drive term

$$H' = \frac{\Omega}{2}(b^\dagger + b). \tag{17}$$

For the Raman process, we are interested in the transition between dressed states $\big|\bar{f0}\big\rangle$ and $\big|\bar{g1}\big\rangle$, which correspond to states $\big|\Phi_2^+\big\rangle$ and $\big|\Phi_1^-\big\rangle$, as defined in Eqn. (15,16). The transition strength up to 1^{st} order in Ω is given by the corresponding matrix element of H'

$$\tilde{g} = \big\langle \bar{f0}\big|H'\big|\bar{g1}\big\rangle = \frac{\Omega\sqrt{2}}{2}\cos(\alpha_2)\sin(\alpha_1) - \frac{\Omega}{2}\cos(\alpha_1)\sin(\alpha_2). \tag{18}$$

This expression for the coupling strength, is one of the main results of this thesis. In the limit where the detuning δ_n is much smaller than the qubit-resonator coupling strength $g\sqrt{n}$, the Raman transition strength $\tilde{g}$ reduces to the simple expression

$$\tilde{g} = \frac{\Omega\sqrt{2}}{2}\alpha_1 - \frac{\Omega}{2}\alpha_2 = g\Omega\frac{\alpha\sqrt{2}}{2}\left(\frac{1}{\delta q + \alpha} - \frac{1}{\delta q}\right) = g\Omega\frac{\alpha}{\sqrt{2}\delta q(\delta q + \alpha)}. \tag{19}$$

[10] In order to use time independent perturbation theory, we transform our Hamiltonian to the rotating frame of the drive frequency ω (See Appendix A).

As anticipated in the introduction, the deconstructive interference between the two Raman transition paths gives us a smaller coupling strength $\tilde{g}$ than the coupling strength associated with either of the paths. Moreover, the anharmonicity, α, that differentiates between the coupling strengths of the two paths plays as important of a role in the magnitude of $\tilde{g}$ as the drive strength Ω and the qubit-resonator coupling g.

4.1.1 Fidelity of the Raman Transition

The fidelity of a transition between two states is defined as the amplitude population oscillations for either of the states. We calculate the amplitude of these oscillations using the time evolution operator

$$U(t) = e^{-iHt},$$

where H is the Hamiltonian for the whole system. If the system is initially in state $\big|\Psi_i\big\rangle$, the population in the initial state for consequent times is given by

$$P_\Psi(t) = \Big|\big\langle \Psi_i \big| \Psi_i(t) \big\rangle\Big|^2,$$

where $\big|\Psi_i(t)\big\rangle = e^{-iHt}\big|\Psi_i\big\rangle$. As a result, the fidelity of the Raman transition can be found to be (See Appendix C)

$$\mathrm{F} = 2 \times 2\big|\alpha_n\big|^2\big|\alpha_m\big|^2, \tag{20}$$

where $\big|\alpha_n\big|$ and $\big|\alpha_m\big|$ are the two largest overlaps between the initial state $\big|\Psi_i\big\rangle = \big|\bar{f0}\big\rangle$ and the eigenstates of the driven system.

Consequently, we need to calculate the coefficients $\alpha_{\bar{f0}\pm}$ in the expansion of the eigenstates of the driven system $\big|\Phi_\pm\big\rangle$. We approach the problem perturbatively on the eigenbasis of the Jaynes-Cummings Hamiltonian as in the last section. However, we need to be careful because we have two distinct sets of states:

1. Nearly degenerate set of states (i.e. the dressed states $\big|\bar{f0}\big\rangle$ and $\big|\bar{g1}\big\rangle$). The interaction due to the external drive $\Omega(a^\dagger + a)$ will give rise to up to first order corrections to the dressed state $\big|\bar{f0}\big\rangle$.

2. The set of states whose energies are quite different than the ones in the nearly degenerate set (NDS). They will give 2^{nd} order corrections to the dressed state $\big|\bar{f0}\big\rangle$.

A treatment to the stated problem is given in [17]. We first treat the set of nearly degenerate states ($\big|\bar{f0}\big\rangle$ and $\big|\bar{g1}\big\rangle$), and then calculate the second order corrections due to the rest of the states ($\big|\bar{e0}\big\rangle$, $\big|\bar{h0}\big\rangle$, and $\big|\bar{e1}\big\rangle$). According to degenerate perturbation theory, the solution for the 2-fold degenerate problem is acquired by solving the Hamiltonian restricted to the NDS:

$$H_{NDS} = \begin{pmatrix} E_{\bar{f0}} + \chi_{\bar{f0}} & \tilde{g} \\ \tilde{g}* & E_{\bar{g1}} + \chi_{\bar{g1}}, \end{pmatrix} \tag{21}$$

where $E_{\bar{f0}/\bar{g1}}$ are the energies of the dressed states $\big|\bar{f0}\big\rangle$ and $\big|\bar{g1}\big\rangle$ and $\chi_{\bar{f0}/\bar{g1}}$ are the respective AC Stark shifts due to states not included in the nearly degenerate set. An important point to keep in mind is that since the dressed states, $\big|\bar{f0}\big\rangle$ and $\big|\bar{g1}\big\rangle$, are exact eigenstates of

the Jaynes-Cummings Hamiltonian, there is no 2^{nd} order process connecting them[11]. For the sake of simplicity, we consider the case of perfect degeneracy (i.e. $E_{\bar{f}0} + \chi_{\bar{f}0} = E_{\bar{g}1} + \chi_{\bar{g}1}$), which is easily achievable using the experimental parameters ω_q and δ_q as in Eqn. (14). In the case of perfect degeneracy the eigenfunctions of the nearly degenerate set ($\left|\bar{f}0\right\rangle$ and $\left|\bar{g}1\right\rangle$) can be found to be [12]

$$\left|\Phi^{\pm}\right\rangle = \frac{1}{\sqrt{2}}\left(\left|\bar{f}0\right\rangle \pm \left|\bar{g}1\right\rangle\right). \tag{23}$$

Eqn. (23) includes corrections up to 1^{st} order consistent with H_{NDS} which includes corrections up to 2^{nd} order. If we stop our approximation scheme here, the values of $\alpha_+ = \left|\left\langle\Phi^+\middle|\bar{f}0\right\rangle\right|$ and $\alpha_- = \left|\left\langle\Phi^-\middle|\bar{f}0\right\rangle\right|$ are both equal to $1/\sqrt{2}$ and the fidelity of the Raman transition, F = 1, by Eqn. (20). Since this result does not explain the results of numerical simulations discussed below, we extend the perturbation theory to the 2^{nd} order for the eigenfunctions $\left|\Phi^{\pm}\right\rangle$.

As mentioned above, we are only interested in the coefficient of the state $\left|\bar{f}0\right\rangle$ in the eigenfunctions $\left|\Phi^{\pm}\right\rangle$ of the driven system. The 2^{nd} order correction modifies the coefficient $\alpha_{\pm} = 1/\sqrt{2}$ in the following way (See Appendix B)

$$\alpha_{\pm} = 1/\sqrt{2} \rightarrow \alpha_{\pm} = \frac{1}{\sqrt{2}}\left(1 - \frac{1}{2}\left(\frac{\sqrt{2}\Omega/2}{\delta q + \alpha}\right)^2 - \frac{1}{2}\left(\frac{\sqrt{3}\Omega/2}{\delta q + 2\alpha}\right)^2\right). \tag{24}$$

Note that the corrections are in order to ensure normalization of $\left|\Phi^{\pm}\right\rangle$ up to 2^{nd} order in perturbation, and they correspond to the population that has leaked from the initial $\left|\bar{f}0\right\rangle$ state to the neighboring $\left|\bar{e}0\right\rangle$ and $\left|\bar{h}0\right\rangle$ states.

To obtain the final result for the fidelity of the Raman transition, we plug in $\alpha_{\pm}$ into Eqn. (20). Thus,

$$\mathrm{F} = 1 - 2\left(\left(\frac{\sqrt{2}\Omega/2}{\delta q + \alpha}\right)^2 + \left(\frac{\sqrt{3}\Omega/2}{\delta q + 2\alpha}\right)^2\right). \tag{25}$$

This approximation for the fidelity of Raman transitions is a main result of this thesis, and it offers an intuitive way to think about what limits the fidelity of the transition. F is lowered due to the population leakage from the states in the NDS to the neighboring states. An immediate consequence of Eqn. (25) is that the Raman process will have higher fidelity if the qubit-drive detuning $\delta_q \leqslant 0$, because the anharmonicity α is always negative. Thus, we need to choose δ_q such that $\delta_q \leqslant 0$, but not too large to reduce $\tilde{g}$ to impractical values. However, since the fidelity decreases more slower than $\tilde{g}$ with respect to δ_q, one can have large fidelity transitions for reasonable $\tilde{g}$.

[11] The matrix element for the 2^{nd} order process is given as

$$\sum_{l=e0,e1} \frac{\left\langle\bar{f}0\middle|H'\middle|\bar{n}\right\rangle}{\left\langle\bar{n}\middle|H'\middle|\bar{g}1\right\rangle}, \tag{22}$$

which vanishes because the pairs $(\left|\bar{f}0\right\rangle, \left|\bar{e}1\right\rangle)$ and $(\left|\bar{g}1\right\rangle, \left|\bar{e}0\right\rangle)$ are no longer coupled by the Jaynes-Cummings interaction.

[12] See Appendix B for the solution for near degeneracy

5 Numerical Simulations

We also conducted numerical simulations to test the limits of the theory presented in the previous section. In particular, we would like to demonstrate the dependencies, $\tilde{g} \propto \Omega$ and $\mathrm{F} \propto \Omega^2$.

The quantities $\tilde{g}$ and F can be determined directly from the time evolution of the $\big|\widetilde{f0}\big\rangle$ population, which is described by Eqn. (69). The time evolution can also be numerically computed using the equation of motion (EOM) for the density matrix [13] The EOM of a density matrix ρ under a unitary Hamiltonian is a 1^{st} order differential equation given by

$$\dot{\rho} = -i\big[\rho, H\big]; \qquad \rho(t=0) = \rho_0. \tag{26}$$

In order to extract the population of a state generic state, $\big|\Psi\big\rangle$, using the density matrix, we simply take the trace[14]

$$P_\Psi = \mathrm{Tr}[\rho(t)\big|\Psi\big\rangle\big\langle\Psi\big|]. \tag{27}$$

The expression in Eqn. (27) depends on the same variables as the Hamiltonian in Eqn. (1): ω_d, Ω, g, and α.

5.1 First Order Couplings and Stark Shifts

The algorithm that we used to solve Eqn. (26) is as follows. We first set the qubit coupling constant g, and the qubit anharmonicity α according to the measurements described in Section 3. A typical value for $\alpha/2\pi$ is 400 MHz and 100 MHz for $g/2\pi$. Since we would like to demonstrate $\tilde{g}(\Omega)$ and $\mathrm{F}(\Omega)$, the only parameter left to be determined is the drive frequency ω_d.

As discussed earlier, the Raman process transition occurs with highest fidelity when the drive frequency ω_d compensates for the frequency difference between $\big|\bar{g1}\big\rangle$ and $\big|\bar{f0}\big\rangle$ levels, including the AC Stark shifts. Thus,

$$\omega_d = 2\omega_q + \alpha - \omega_r + \Delta_{AC}, \tag{28}$$

where Δ_{AC} is the difference between the AC Stark shifts $(\chi_{\bar{f0}} - \chi_{\bar{g1}})$ of $\big|\bar{g1}\big\rangle$ and $\big|\bar{f0}\big\rangle$. The AC Stark shifts are approximately given by[15]

$$\chi_{f0} = \left|\frac{\Omega}{2}\right|^2 \left(\frac{2}{\delta_q + \alpha} - \frac{3}{\delta_q + 2\alpha}\right) - \left|\frac{2g^2}{\delta_q}\right| \tag{29}$$

$$\chi_{g1} = -\left|\frac{\Omega}{2}\right|^2 \frac{1}{\delta_q} + \left|\frac{g^2}{\delta_q + \alpha}\right|, \tag{30}$$

After numerically computing $P_{\bar{f0}}$, for different drive powers Ω, each trace is fit to a single cosine function (Fig. 10).

[13] However, in the absence of dissipation, the system can be described with only pure states. Thus the density matrix formalism is not necessary.

[14] Note that th trace, $\mathrm{Tr}[\cdots]$ is like the dot product in the operator space. In other words, the trace operation can be though as measuring the overlap between the density operator and the state $\big|\Psi\big\rangle$.

[15] The exact shift that we used for the simulations were optimized to give highest fidelity at small drive strengths Ω. Implementing a correction for the AC Stark shifts is complicated because the shifts depend on δ_q, δ_r, and Ω, exhausting the experimentally tunable parameters.

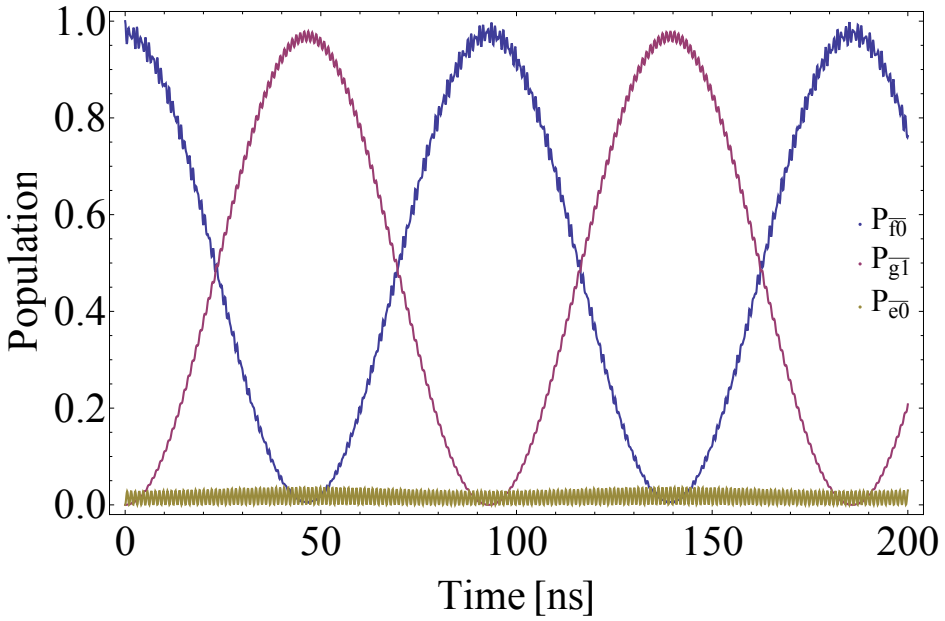

Figure 10: Time evolution of the $\left|f0\right\rangle$, $\left|g1\right\rangle$, and $\left|e1\right\rangle$ states. The traces were produced by sampling the solution to Eqn. (26) with initial state $\left|\Psi_i\right\rangle \equiv \left|\overline{f0}\right\rangle$.

The fitting parameters give us the strength ($2\tilde{g}$) and the fidelity of the Raman transition. The dependence of $2\tilde{g}$ and F on the drive strength Ω can be seen in Fig. 11 and 12 . The results are in good agreement the theoretical predictions, for $\frac{\Omega}{\delta_q}^2 \ll 1$, as expected. The approximation seem to break down as $\Omega/2\pi$ is increased above 250 MHz. For experimentally reasonable values of $g/2\pi$ = 100 MHz and $\delta_q/2\pi$ = -600 MHz, we found that the fidelity of the transition is lower than 90 percent for $\tilde{g}/2\pi \geq 10$ MHz. The fit curve in Fig. 11 also takes into account corrections up to 3^{rd} order in the drive strength Ω.

6 Conclusion and Outlook

In this thesis, we have realized a Raman transition in a superconducting circuit QED architecture. The expressions for the fidelity and the strength Raman transition can be derived straightforwardly from 1^{st} order degenerate perturbation theory [16] . As anticipated in the introduction, the rate of Raman transition suffers from the qubit-resonator detuning and the destructive interference between the two transition paths connecting $\left|\bar{f}0\right\rangle$ and $\left|\bar{g}1\right\rangle$ states. This interference results in a coupling strength $\tilde{g}$ linearly dependent on anharmonicity, α, which differentiates between the two Raman transition paths.

We also determined that the fidelity of Raman transition depends on the population leakage from the initial state $\left|\bar{f}0\right\rangle$ to neighboring states other than $\left|\bar{g}1\right\rangle$ (Eqn. (25)). Another implication of this result is that the Raman transition has better fidelity for qubit frequency above the resonator, $\delta q \leqslant 0$, since anharmonicity is always negative.

[16] The 1^{st} order perturbation theory is also applicable to simpler systems, such as the Λ configuration in the atomic physics experiments. Importantly, unlike the adiabatic elimination method, the perturbative approach also gives approximations for the population of the intermediate state and the fidelity of transitions.

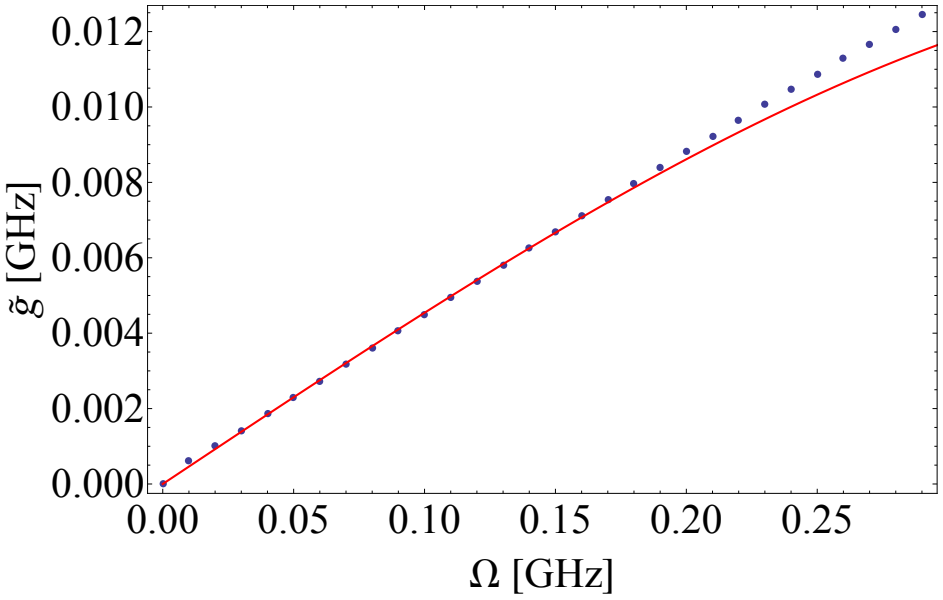

Figure 11: The dependence of the Raman transition coupling strength $\tilde{g}$ on the drive strength Ω. The data points are the values of $\tilde{g}(\Omega)$ extracted from the numerical simulations. The fit curve, also takes account of the effect of first order interactions on the strength of the second order interaction $\tilde{g}$

Thus, one needs to choose the experimental parameters such that $\tilde{g}$ is much faster than the decay rate of the qubit and the fidelity of Raman process is still reasonable for applications discussed in the introduction. Our numerical simulations show that for a $\tilde{g}/2\pi$ of 10 MHz, the maximum fidelity is about 0.90.

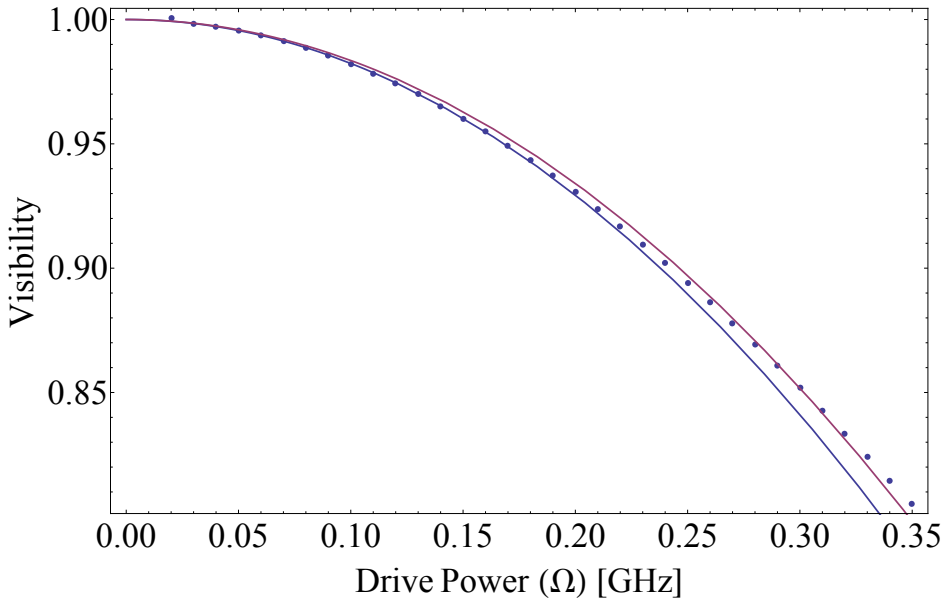

Figure 12: The dependence of the visibility of Raman process transition on the drive strength Ω. The data points are the values of fidelity extracted from the numerical simulations. The fit curve is shown in red and Eqn. (25) in blue.

Appendix A Qubit-Resonator Energy Level Diagram in a Rotating Frame

In this section we will transform the Hamiltonian

$$H/\hbar = \omega_q \hat{n}_q + \alpha b^\dagger b^\dagger b b + \omega_r \hat{n}_r + \Omega \cos(\omega_d t + \phi)(b + b^\dagger) + g(b a^\dagger + b^\dagger a), \tag{31}$$

to a time-independent form by going to the frame of reference rotating with the frequency of the external drive, ω_d. The time independent Hamiltonian is useful because we can then use simpler time-independent perturbation theory to analyze it. The desired gauge transformation is

$$U(t) = e^{-i\omega_d \hat{n} t}, \tag{32}$$

where $\hat{n}$ is the number operator that counts the total number of excitations associated with a state.

The transformation of the Hamiltonian under a time dependent transformation is given by

$$\tilde{H} = UHU^\dagger - iU\dot{U}^\dagger. \tag{33}$$

Thus, using Eqn. (32), we obtain the Hamiltonian in the rotating frame

$$\tilde{H} = UHU^\dagger - \omega_d \hat{n}. \tag{34}$$

Notice that this transformation can also be thought as going to the interaction picture of the time-independent Hamiltonian, $\omega_d \hat{n}$. As a result of the transformation, each basis state of the Hamiltonian is shifted down in energy by an amount dependent on its total number of excitations. While the energy of the state, E_{g0} will not change under the transformation since it has no excitations, the energy of the state E_{g1} will be lowered by ω_d and energy of the state E_{e1} will be lowered by $2\omega_d$ and so on (Fig. 13).

The action of the transformation on the raising and the lowering operators are given by

$$\tilde{b}^+ = b^+ e^{i\omega_d t} \tag{35}$$
$$\tilde{b}^- = b^- e^{-i\omega_d t} \tag{36}$$
$$\tilde{a}^\dagger = a^\dagger e^{i\omega_d t} \tag{37}$$
$$\tilde{a} = a e^{-i\omega_d t}. \tag{38}$$

With the relations above, it is clear that any operator that has the same number of creation and annihilation operators of any type will be invariant under the transformation $U(t)$. The only term that will be effected is the time dependent drive term, which, by setting $\phi = 0$ becomes

$$\begin{aligned} & U(t)\left(\Omega \cos(\omega_d t + \phi)(b + b^+)\right) U^{-1}(t) \\ = \;& \Omega \frac{e^{\omega_d t} + e^{-\omega_d t}}{2}(b e^{-i\omega_d t} + b^+ e^{i\omega_d t}) \\ = \;& \frac{\Omega}{2}(b + b^+) + \frac{\Omega}{2}(b e^{-i2\omega_d t} + b^+ e^{i2\omega_d t}). \end{aligned} \tag{31}$$

Lastly, we eliminate the terms which are evolving much faster than all the other terms in the Hamiltonian[17], and the Hamiltonian of the perturbed system in the rotating frame is approximated by

$$H/\hbar \cong \delta q \hat{n}_q + \alpha b^\dagger b^\dagger b b + \delta_r \hat{n}_r + g(ba^\dagger + b^\dagger a) + \frac{\Omega}{2}(b + b^\dagger), \tag{40}$$

where $\delta_{q(r)} = \omega_{q(r)} - \omega_d$. The resulting energy level diagram of the Hamiltonian in the rotating frame is shown in Fig. 13.

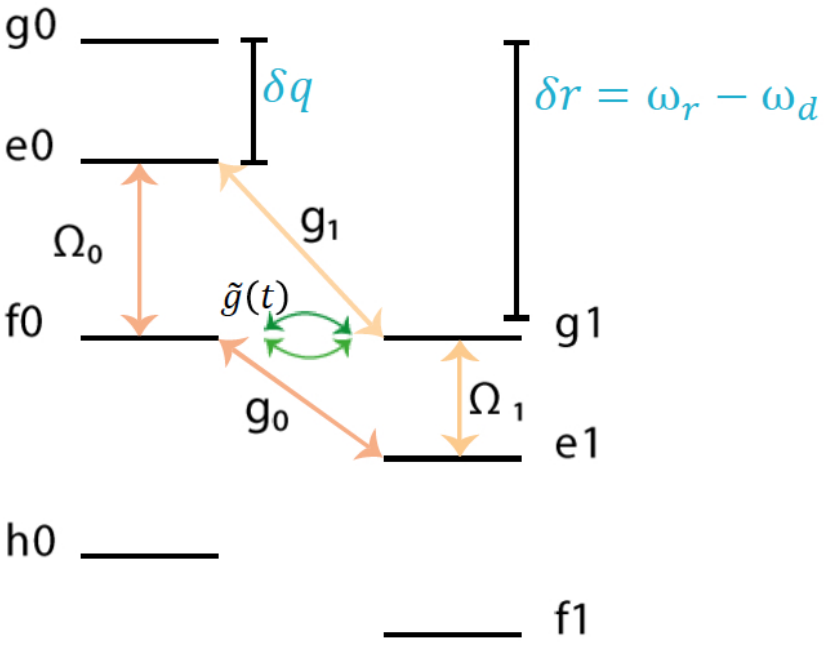

Figure 13: The energy level diagram for the qubit-resonator system in the rotating frame of the drive ω_d. The fast oscillating parts of the system are integrated out by applying the rotating wave approximation.

In the energy level diagram depicted in Fig. 13, the separation between the levels corresponds to the detuning between the transition frequencies and the drive frequency ω_d. We should remember that, according to Eqn. (51), we need to satisfy $\left(\frac{\Omega_0}{\delta q}\right)^2 \cong \left(\frac{\Omega/2}{\delta q}\right)^2 \ll 1$ in order to ensure the validity of the 2^{nd} order time independent perturbation theory. In general, for the general perturbation theory on many states, one should make sure that the largest ratio $\left(\frac{\Omega_i}{\delta_i}\right)^2 \ll 1$.

[17]This step is commonly called the rotating wave approximation. Upon begin integrated over time coordinate, the exponent of the factor $e^{-i2\omega_d t}$ will go to the denominator.

$$\int dt e^{-i2\omega_d t} = \frac{e^{-i2\omega_d t}}{i2\omega_d t} \tag{39}$$

Appendix B Time Independent Perturbation Theory [18]

B.1 Nondegenerate Perturbation Theory

The main tool that we use to analyze the Raman transition is the time independent perturbation theory. To begin with, we write our system's Hamiltonian as a sum of an unperturbed operator H_0, and a perturbation operator V:

$$H = H_0 + V. \tag{41}$$

The eigenstates of the unperturbed operator are assumed to be known. These eigenstates will be used as the basis we construct our perturbation theory on. For now, we only consider non-degenerate bases. The basis states are defined by the equation,

$$H_0\big|\Psi^{(0)}\big\rangle = E^{(0)}\big|\Psi^{(0)}\big\rangle. \tag{42}$$

Consequently, the equation whose eigen-system we would like to approximate is

$$H\big|\Psi\big\rangle = (E^0 + V)\big|\Psi\big\rangle = E\big|\Psi\big\rangle. \tag{43}$$

To start with, we expand the eigenfunctions of the Hamiltonian in Eqn. (41) in the basis of unperturbed eigenfunctions:

$$\big|\Psi\big\rangle = \sum_n c_n\big|\Psi_n^{(0)}\big\rangle. \tag{44}$$

Substituting this expansion to Eqn. (41) and projecting it onto the unperturbed eigenstate $\big|\Psi_k\big\rangle^{(0)}$, we re-write the Schoedinger equation in the basis of unperturbed eigenstates

$$(E - E_k^{(0)})c_k = \sum_n V_{kn}c_n, \tag{45}$$

where V_{nk} are the matrix elements of the perturbation operator defined by

$$V_{nk} = \big\langle\Psi_n^{(0)}\big|V\big|\Psi_k^{(0)}\big\rangle. \tag{46}$$

We then seek the solution to the Eqn. (45) in the following form:

$$c_k = c_k^{(0)} + c_k^{(1)} + c_k^{(2)} + \cdots \qquad E = E^{(0)} + E^{(1)} + E^{(2)} + \cdots. \tag{47}$$

In order to determine the correction to the n^{th} eigenvalue and eigenfunction, we set the initial configuration to $c_n^0 = 1$ and $c_m^0 = 0$ for all $m \neq n$. To determine the first order approximation, we need to expand the solution only to the first order: $E = E_n^{(0)} + E_n^{(1)}$ and $c_k = c_k^{(0)} + c_k^{(1)}$. Plugging these expansions in Eqn. (45) and retaining only the first order terms gives us the familiar correction to the energy for $n = k$

$$E^{(1)} = V_{nn} = \big\langle\Psi_n^{(0)}\big|V\big|\Psi_n^{(0)}\big\rangle; \tag{48}$$

and the first order correction to the c_n for $n \neq k$

$$c_k^{(1)} = \frac{V_{kn}}{E_n^{(0)} - E_k^{(0)}}. \tag{49}$$

Thus, keeping terms up to the first order in our perturbation theory, the normalized eigenstate of the perturbed Hamiltonian is

$$\big|\Psi\big\rangle \cong \big|n^0\big\rangle + \sum_k{}' c_k^{(1)} \big|k^0\big\rangle, \tag{50}$$

where the primed summation omits terms with $c_n^{(1)}$. Note that the validity of the 1st order perturbative treatment depends mainly on the condition that c_k's are smaller than unity. Thus,

$$\frac{V_{kn}}{E_n^{(0)} - E_k^{(0)}} \ll 1. \tag{51}$$

Using the 1st order correction coefficients of the wavefunction, we obtain the 2nd order correction in the eigenenergy.

$$E_n^{(2)} = \sum_m \frac{\big|V_{nm}\big|^2}{E_n^{(0)} - E_m^{(0)}}. \tag{52}$$

Eqn. (52) will gives us the "AC Stark shift" correction to the energies for a periodically driven system described in the suitable rotating frame.

B.2 Degenerate Perturbation Theory

We have seen that in the rotating frame, the initial ($\big|\bar{f}0\big\rangle$) and the final ($\big|\bar{g1}\big\rangle$) of the Raman transition need to be nearly degenerate to ensure the highest fidelity of the transition. Let us build a perturbation theory for such a system. Notice that the corrections given by Eqn. (49) diverge when the unperturbed eigenstates are degenerate, so we need a slightly different approach.

The starting point for the analysis is still Eqn. (45), which is the Schrödinger's equation written in the eigenbasis of the unperturbed states. We then equate $k = n, n', \cdots$, where $n, n', \cdots$ indexes the nearly degenerate states (NDS). We set the initial conditions as initially set, $c_n = c_n^{(0)}$, for the states in NDS, and $c_m^{(0)} = 0$, for states not in the NDS. Plugging these conditions in Eqn. (45), we obtain

$$\sum_{n'} (V_{nn'} - E_{n'}^{(1)} \delta_{nn'}) c_{n'}^{(0)} = 0, \tag{53}$$

which has a solution only if the "secular equation" is satisfied:

$$\big|V_{nn'} - E_{n'}^{(1)} \delta_{nn'}\big| = 0. \tag{54}$$

The solutions to Eqn. (54) give us the first order correction to the energies in degenerate perturbation theory. Also note that substituting the solutions of the "secular equation" in Eqn. (53), it is possible to calculate the expansion coefficients $c_{n'}^0$. Lastly, we see that unless the "secular equation" has repeating roots, the degeneracy of the unperturbed system will be destroyed.

Next, we would like to write the like of Eqn. (54) for the second order correction to the energies of the degenerate system, for this is exactly what we used to analyze the Raman transition. In order to obtain the desired result, we first need to assume that we can select

a basis in which the first order correction on the degenerate energies, $E^{(1)}$ is zero. Thus, we can expand the energies of the perturbed system as $E = E^{(0)} + E^{(2)}$, and $c_n = c_n^{(0)}$, for the first order correction is vanishing. Also, as before, we set $c_m^{(0)} = 0$ for m no in NDS.

We plug these initial conditions in Eqn. (45) to get the second order correction to the degenerate energies:

$$E^{(2)} c_n^{(0)} = \sum_m V_{nm} c_m^{(1)}. \tag{55}$$

On the other hand, if $k = m$ not in NDS, we get the first order correction to the degenerate eigenstates

$$\left(E_n^{(0)} - E_m^{(0)}\right) c_m^{(1)} = \sum_{n'} V_{mn'} c_{n'}^{(0)}, \tag{56}$$

hence

$$c_m^{(1)} = \sum_{n'} \frac{V_{mn'}}{\left(E_n^{(0)} - E_m^{(0)}\right)} c_{n'}^{(0)}. \tag{57}$$

Plugging Eqn. (57) into Eqn. (55), we obtain the secular equation for the second order degenerate transitions

$$\left| \sum_m \frac{V_{nm} V_{mn'}}{E_n^{(0)} - E_m^{(0)}} - E^{(2)} \delta_{nn'} \right| = 0. \tag{58}$$

The solutions to Eqn. (58) give us the second order correction to the energies of the degenerate states. Notice that Eqn. (54) and Eqn. (58) are identical if we proposed

$$V_{nn'}^{(2)} \equiv \sum_m \frac{V_{nm} V_{mn'}}{E_n^{(0)} - E_m^{(0)}}. \tag{59}$$

Eqn. (59) gives us the second order coupling strength between two degenerate states. Finally, we note that in the case that there are only two degenerate states, $\left|n\right\rangle$ and $\left|m\right\rangle$, in the unperturbed system, the eigenstates of the perturbed system are given by $\left|\Psi\right\rangle = c_n^0 \left|n\right\rangle + c_m^0 \left|m\right\rangle$, where

$$c_1^{(0)} = \left(\frac{V_{nn'}^{(2)}}{2\left|V_{nn'}^{(2)}\right|} \left(1 \pm \frac{V_{nn}^{(2)} - V_{n'n'}^{(2)}}{\sqrt{(V_{nn}^{(2)} - V_{n'n'}^{(2)})^2 + 4\left|V_{nn'}^{(2)}\right|^2}} \right) \right)^{1/2}, \tag{60}$$

$$c_2^{(0)} = \pm \left(\frac{V_{nn'}^{(2)}}{2\left|V_{nn'}^{(2)}\right|} \left(1 \mp \frac{V_{nn}^{(2)} - V_{n'n'}^{(2)}}{\sqrt{\left(V_{nn}^{(2)} - V_{n'n'}^{(2)}\right)^2 + 4\left|V_{nn'}^{(2)}\right|^2}} \right) \right)^{1/2}, \tag{61}$$

with energies,

$$E^{\pm} = 1/2 \left(V_{nn}^{(2)} + V_{n'n'}^{(2)} \pm \sqrt{V_{nn}^{(2)} - V_{n'n'}^{(2)} + 4\left|V_{nn'}^{(2)}\right|^2} \right), \tag{62}$$

where $V_{nn}^{(2)}$ is the AC Stark shift induced on the n^{th} state by the states not in NDS, and $V_{nn'}^{(2)}$ is the effective second order coupling between n^{th} and n'^{th} levels as given in Eqn. (59).

Appendix C Fidelity of Transitions

We define the fidelity, F, of the transition between the states $|n\rangle$ and $|n'\rangle$ as the visibility (amplitude) of Rabi oscillations between them.

To this end, let us consider a generic Hamiltonian H, the time evolution operator, $U(t)$, is given by ($\hbar = 1$)

$$U(t) = e^{-iHt}. \tag{63}$$

An initial state $|\Psi_i\rangle$ will then evolve accordingly:

$$|\Psi_i(t)\rangle = e^{-iHt}|\Psi_i(0)\rangle \equiv e^{-iHt}|\Psi_i\rangle. \tag{64}$$

In order to see the Rabi oscillations in the population of $|\Psi_i\rangle$, we would like to project the propagated state $|\Psi_i(t)\rangle$ back on the initial state $|\Psi_i\rangle$. Thus, the time evolution of the population in $|\Psi_i\rangle$ is given by

$$P_\Psi(t) = \left|\langle\Psi_i|\Psi_i(t)\rangle\right|^2. \tag{65}$$

Next, we expand the initial state in the eigenbasis of the driven system,

$$|\Psi_i(0)\rangle = \sum_n \alpha_n|n\rangle, \tag{66}$$

where the extension coefficients α_n's are the overlaps between the initial state and the eigenstates of the driven system:

$$\langle n|\Psi_i\rangle = \alpha_n. \tag{67}$$

Plugging this extension in Eqn. (64), we obtain,

$$|\Psi_i(t)\rangle = e^{-iHt}\sum_n \alpha_n|n\rangle = \sum_n e^{-i\epsilon_n t}\alpha_n|n\rangle. \tag{68}$$

Thus, the evolution of the $|\Psi_i\rangle$ population can be calculated to be

$$\left|\langle\Psi_i|\Psi_i(t)\rangle\right|^2 = \sum_n |\alpha_n|^4 + 2\sum_{n\geqslant m} |\alpha_n|^2|\alpha_m|^2\cos\left((\epsilon_n - \epsilon_m)t\right), \tag{69}$$

where $|\alpha_n|^2$'s represent the percentage of the initial state population distributed among the eigenstates $|n\rangle$ once the perturbation is turned on, and ϵ_n and ϵ_m are the energies of the eigenstates of the driven system which overlaps with the initial state $|\Psi_i\rangle$.

Eqn. (69) gives us direct access to the fidelity and the strength of any transition induced by the external drive. The fidelity of the transition between $|\Psi_i\rangle$ and another unperturbed eigenstate[18] is simply given by

[18]The compositions of these eigenstates cannot be known without treating the full Hamiltonian. However, we note that in the case of full Rabi oscillations where $|\alpha_n|^2 = 1/2$, $|\alpha_m|^2 = 0$ or $\pm 1/\sqrt{2}$ for $m \neq n$. One can also see the factor $|\alpha_n|^2|\alpha_m|^2$ as the square of the coherence between the two eigenstates of the driven system mediated through the initial state $|\Psi_i\rangle$.

$$\text{Fidelity} = 2 \times 2\left|\alpha_n\right|^2\left|\alpha_m\right|^2, \tag{70}$$

where $\left|\alpha_n\right|$ and $\left|\alpha_m\right|$ are the two largest overlaps between the initial state $\left|\Psi_i\right\rangle$ and the eigenstates of the driven system. The strength of the transition is given by the difference in energy between the eigenstates $\left|n\right\rangle$ and $\left|m\right\rangle$.

References

[1] J. I. Cirac, P. Zoller, H. J. Kimble, and H. Mabuchi, Phys. Rev. Lett. **78**, 3221 (1997)

[2] H. J. Kimble, Nature **435**, 1023 (2008)

[3] Bose S., Carollo A., Fuentes-guridi I., Santos M. F. and Vedral V., (2003) Journal of Modern Optics **50**, 1175-1181

[4] M. Pechal, S. Berger, A. A. Abdumalikov, Jr., J. M. Fink, J. A. Mlynek, L. Steffen, A. Wallraff, and S. Filipp, Phys. Rev. Lett. 108, 170401 (2012)

[5] S. Berger, M. Pechal, S. Pugnetti, A. A. Abdumalikov, Jr., L. Steffen, A. Fedorov, A. Wallraff, and S. Filipp, Phys. Rev. B 85, 220502(R) (2012)

[6] Fuentes-Guridi I., Carollo A., Bose S. and Vedral V., (2002) Phys. Rev. Lett. **89** 220404

[7] Roee Ozeri, Tutorial: The trapped-ion qubit toolbox (2011), arXiv:1106.1190

[8] P. M. Radmore and P. L. Knight (1982), J. Phys. B: At. Mol. Phys. **15** 561-573

[9] Gerry C. C. and Eberly J. H. (1990) Phys. Rev. A 42(11) 6805-6815

[10] Law C. K. and Kimble H. J., (1997) J. Mod **44** 2067

[11] Brion E, Molmer K and Saman M 2007 Phys. Rev. Lett. **99** 260501

[12] Rui Han, Hui Khoon Ng, Berthold-Georg Englert (2013), Journal of Modern Optics, 255-265

[13] R. Bianchetti, S. Filipp, M. Baur, J. M. Fink, M. Goeppl, P. J. Leek, L. Steffen, A. Blais, and A. Wallraff, Physical Review A **80**, 043840 (2009)

[14] D. Bozyiğit, C. Lang et. al., Nature Physics **7**, 154 (2011)

[15] J. Koch, T. Yu et. al., Phys. Rev. A **76**, 042319 (2007)

[16] J. Majer, J. M. Chow, J. M. Gambetta, Jens Koch, B. R. Johnson, J. A. Schreier, L. Frunzio, D. I. Schuster, A. A. Houck, A. Wallraff, A. Blais, M. H. Devoret, S. M. Girvin and R. J. Schoelkopf (2007), Nature **449**, 443-447

[17] M.S. Dresselhaus "Optical Properties of Solids" , Lecture notes

[18] L.D. Landau, E.M. Lifshitz (1977). Quantum Mechanics: Non-Relativistic Theory. Vol. 3 (3rd ed.). Pergamon Press.